

Jorge G. Zornberg, The University of Texas at Austin

## ADVANCES IN REINFORCED SOIL TECHNOLOGY

---

**ABSTRACT:** Traditional soil reinforcing techniques involve the use of continuous geosynthetic inclusions such as geogrids and geotextiles. The acceptance of geosynthetics in reinforced soil construction has been triggered by a number of factors, including aesthetics, reliability, simple construction techniques, good seismic performance, and the ability to tolerate large deformations without structural distress. Following an overview of conventional reinforced soil applications, this paper focuses on recent advances in reinforced soil technology. Examples include advances in reinforced soil design for conventional loading (e.g. validation of analysis tools), advances in design for unconventional loading (e.g., reinforced bridge abutments), and advances in reinforcement materials (e.g., polymeric fiber reinforcements).

### 1 INTRODUCTION

Geosynthetic inclusions within a soil mass can provide a reinforcement function by developing tensile forces which contribute to the stability of the geosynthetic-soil composite (a reinforced soil structure). Design and construction of stable slopes and retaining structures within space constraints are aspects of major economical significance in geotechnical engineering projects. For example, when geometry requirements dictate changes of elevation in a highway project, the engineer faces a variety of distinct alternatives for designing the required earth structures. Traditional solutions have been either a concrete retaining wall or a conventional, relatively flat, unreinforced slope (Figure 27.2). Although simple to design, concrete wall alternatives have generally led to elevated construction and material costs. On the other hand, the construction of unreinforced embankments with flat slope angles dictated by stability considerations is an alternative often precluded in projects where design is controlled by space constraints.

Geosynthetics are particularly suitable for soil reinforcement. Geosynthetic products typically used as reinforcement elements are nonwoven geotextiles, woven geotextiles, geogrids, and geocells. Reinforced soil vertical walls generally provide vertical grade separations at a lower cost than traditional concrete walls. Reinforced wall systems involve the use of shotcrete facing protection or of facing elements such as precast or cast-in-place concrete panels. Alternatively, steepened reinforced slopes may eliminate the use of facing elements, thus saving material costs and construction time in relation to vertical reinforced walls. As indicated in **Figure 1** a reinforced soil system generally provides an optimized alternative for the design of earth retaining structures.

A reduced scale geotextile-reinforced slope model built using dry sand as backfill material. The maximum slope inclination of an unreinforced sand under its own weight is the angle of repose of the sand, which is well below the inclination of the slope face of the model. Horizontal geotextile reinforcements placed within the backfill provided stability to the steep sand slope. In fact, not only the reinforced slope model did not fail under its own weight, but its failure only occurred after the unit weight of the backfill was increased 67 times by placing the model in a geotechnical centrifuge (Zornberg et al., 1998).

The use of inclusions to improve the mechanical properties of soils dates to ancient times. However, it is only within the last quarter of century or so (Vidal, 1969) that analytical and experimental studies have led to the contemporary soil reinforcement techniques. Soil reinforcement is now a highly attractive alternative for embankment and retaining wall projects because of the economic benefits it offers in relation to conventional retaining structures. Moreover, its acceptance has also been triggered by a number of technical factors, that include aesthetics, reliability, simple construction techniques, good seismic performance, and the ability to tolerate large deformations without structural distress. The design of reinforced soil slopes is based on the use of limit equilibrium methods to evaluate both external (global) and internal stability of the structure. The required tensile strength of the reinforcements is selected during design so that the margins of safety, considering an internal failure are adequate. Guidance in soil reinforcement design procedures is provided by Elias et al. (2001).

## **2 VALIDATION OF DESIGN TOOLS**

### **2.1 Overview**

The use of inclusions to improve the mechanical properties of soils dates to ancient times. However, it is only within the last three decades or so (Vidal 1969) that analytical and experimental studies have led to the contemporary soil reinforcement techniques. Soil reinforcement is now a highly attractive alternative for embankment and retaining wall projects because of the economic benefits it offers in relation to conventional retaining structures. Moreover, its acceptance has also been triggered by a number of technical factors, which include aesthetics, reliability, simple construction techniques, good seismic performance, and the ability to tolerate large deformations without structural distress. The design of reinforced soil slopes is based on the use of limit equilibrium methods to evaluate both external (global) and internal stability. After adopting the shear strength properties of the backfill material, the required tensile strength of the reinforcements can be defined in the design so that the margin of safety is adequate.

Geosynthetics are classified as extensible reinforcements. Consequently, the soil strength may be expected to mobilize rapidly, reaching its peak strength before the reinforcements achieve their ultimate strength. This rationale has led to some recommendations towards the adoption of the residual shear strength for the design of geosynthetic-reinforced slopes. This is the case of

commonly used design methods such as those proposed by Jewell (1991) and Leshchinsky and Boedeker (1989). Several agencies have endorsed the use of residual shear strength parameters in the design of reinforced soil structures, as summarized in Table 1. Zornberg and Leshchinsky (2001) present a review of current design criteria used by different agencies for geosynthetic-reinforced walls, geosynthetic-reinforced slopes, and embankments over soft soils.

The use of the peak friction angle has been common practice in the US for the design of geosynthetic-reinforced slopes. Guidance in soil reinforcement design procedures has been compiled by several federal agencies in the US, including the American Association of State Highway and Transportation Officials (AASHTO 1996), and the Federal Highway Administration (Elias et al. 2001). Design guidance is also provided by the National Concrete Masonry Association (NCMA 1997), possibly the only industry manual of soil reinforcement practice. The above mentioned design guidance manuals recommend the use of the peak friction angle in the limit equilibrium analyses. Other agencies that have also endorsed the use of peak shear strength parameters in the design of reinforced soil structures are summarized in Table 1.

A hybrid approach was recently proposed by Leshchinsky (2000, 2001). Central to his approach is the use of a design procedure in which peak soil shear strength properties would be used to locate the critical slip surface, while the residual soil shear strength properties would subsequently be used along the located slip surface to compute the reinforcement requirements.

In order to address the controversial issue regarding selection of shear strength properties in reinforced soil design, this paper presents experimental evidence on failed reinforced slopes. Specifically, the experimental information obtained from centrifuge modeling supports the use of peak shear strength parameters in the design of geosynthetic-reinforced soil structures. The perceived conservatism in design is also not supported by the generally observed good performance of monitored reinforced soil structures.

## **2.2 Centrifuge Testing Program**

Limit equilibrium analysis methods have been traditionally used to analyze the stability of slopes with and without reinforcements. However, to date, limit equilibrium predictions of the performance of geosynthetic-reinforced slopes have not been fully validated against monitored failures. This has led to a perceived overconservatism in their design. Consequently, an investigation was undertaken to evaluate design assumptions for geosynthetic-reinforced slopes (Zornberg et al. 1998a, 2000). The results of centrifuge tests provide an excellent opportunity to examine the validity of various assumptions typically made in the analysis and design of reinforced soil slopes. This paper presents the aspects of that study aimed at evaluating the shear strength properties governing failure of reinforced soil slopes.

All reinforced slope models in the experimental testing program had the same geometry and were built within the same strong box. A transparent Plexiglas plate was used on one side of the box to enable side view of the models during testing. The other walls of the box were aluminum

plates lined with Teflon to minimize side friction. The overall dimensions of the geotextile-reinforced slope models are as shown in **Figure 2** for a model with nine reinforcement layers. Displacement transducers are also indicated in the figure.

The number of reinforcement layers in the models ranged from six to eighteen, giving reinforcement spacing ranging from 37.5 mm to 12.5 mm. All models used the same reinforcement length of 203 mm. The use of a reasonably long reinforcement length was deliberate, since this study focused on the evaluation of internal stability against breakage of the geotextile reinforcements. In this way, external or compound failure surfaces were not expected to develop during testing. As shown in the figure, the geotextile layers were wrapped at the slope facing in all models. Green colored sand was placed along the Plexiglas wall at the level of each reinforcement in order to identify the failure surface. In addition, black colored sand markers were placed at a regular horizontal spacing (25 mm) in order to monitor lateral displacements within the backfill material.

The variables investigated in this study were selected so that they could be taken into account in a limit equilibrium framework. Accordingly, the selected variables were:

- Vertical spacing of the geotextile reinforcements: four different reinforcement spacings were adopted;
- soil shear strength parameters: the same sand at two different relative densities was used; and
- ultimate tensile strength of the reinforcements: two geotextiles with different ultimate tensile strength were selected.

Of particular relevance, for the purpose of the issues addressed in this paper, is the fact that that the same sand placed at two different relative densities was used as backfill material for the centrifuge models. The backfill material at these two relative densities has different peak shear strength values but the same residual shear strength.

The model slopes were built using Monterey No. 30 sand, which is a clean, uniformly graded sand classified as SP in the Unified Soil Classification System (Zornberg et al. 1998b). The particles are rounded to subrounded, consisting predominantly of quartz with a smaller amount of feldspars and other minerals. The average particle size for the material is 0.4 mm, the coefficient of uniformity is 1.3, and the coefficient of curvature is about 1.1. The maximum and minimum void ratios of the sand are 0.83 and 0.53, respectively. To obtain the target dry densities in the model slopes, the sand was pluviated through air at controlled combinations of sand discharge rate and discharge height. The unit weights for the Monterey No. 30 sand at the target relative densities of 55% and 75% are 15.64 kN/m<sup>3</sup> and 16.21 kN/m<sup>3</sup>, respectively.

Two series of triaxial tests were performed to evaluate the friction angle for the Monterey No. 30 sand as a function of relative density and of confining pressure. The tests were performed using a modified form of the automated triaxial testing system developed by Li et al. (1988). The

specimens had nominal dimensions of 70 mm in diameter and 150 mm in height and were prepared by dry tamping. Figure 3 shows the stress strain response obtained from the series of tests conducted to evaluate the behavior of Monterey No. 30 sand as a function of relative density. All tests shown in the figure were conducted using a confining pressure of 100 kPa. As can be observed in the figure, while the sand shows a different peak shear strength for different relative densities, the shear stress tends to a single residual shear strength for large strain conditions. Figure 4 shows the increase in peak friction angle with increasing relative density at a confining pressure of 100 kPa. Of particular interest are the friction angles obtained at relative densities of 55% and 75%, which correspond to the relative density of the backfill material in the models. The estimated triaxial compression friction angles ( $\phi_c$ ) at these relative densities are  $35^\circ$  and  $37.5^\circ$ , respectively. Although the tests did not achieve strain values large enough to guarantee a critical state condition, the friction angles at large strains appear to converge to a residual value ( $\phi_r$ ) of approximately  $32.5^\circ$ . This value agrees with the critical state friction angle for Monterey No. 0 sand obtained by Riemer (1992). As the residual friction angle is mainly a function of mineralogy (Bolton 1986), Monterey No. 0 and Monterey No. 30 sands should show similar  $\phi_r$  values. The effect of confining pressure on the frictional strength of the sand was also evaluated. The results showed that the friction angle of Monterey No. 30 decreases only slightly with increasing confinement. The fact that the friction angle of this sand does not exhibit normal stress dependency avoids additional complications in the interpretation of the centrifuge model tests.

Scale requirement for the reinforcing material establish that the reinforcement tensile strength in the models be reduced by  $N$ . That is, an  $N$ th-scale reinforced slope model should be built using a planar reinforcement having  $1/N$  the strength of the prototype reinforcement elements (Zornberg et al. 1998a). Two types of nonwoven interfacing fabrics, having mass per unit area of  $24.5 \text{ g/m}^2$  and  $28 \text{ g/m}^2$ , were selected as reinforcement. Unconfined ultimate tensile strength values, measured from wide-width strip tensile tests ASTM D4595, were  $0.063 \text{ kN/m}$  and  $0.119 \text{ kN/m}$  for the weaker and stronger geotextiles, respectively. Confined tensile strength values, obtained from backcalculation of failure in the centrifuge slope models, were  $0.123 \text{ kN/m}$  and  $0.183 \text{ kN/m}$  for the weaker and stronger geotextiles, respectively (Zornberg et al. 1998b). Confined tensile strength values were used for estimating the factor of safety of the models analyzed in this study under increasing  $g$ -levels.

### 2.3 Typical Centrifuge Test Results

The models were subjected to a progressively increasing centrifugal acceleration until failure occurred. A detailed description of the characteristics of the centrifuge testing program is presented by Zornberg et al. (1998a). The centrifuge tests can be grouped into three test series (B, D, or S). Accordingly, each reinforced slope model in this study was named using a letter that identifies the test series, followed by the number of reinforcement layers in the model. Each test series aimed at investigating the effect of one variable, as follows:

## ZORNBERG • ADVANCES IN REINFORCED SOIL TECHNOLOGY

- Baseline, B-series: Performed to investigate the effect of the reinforcement vertical spacing.
- Denser soil, D-series: Performed to investigate the effect of the soil shear strength on the stability of geosynthetic-reinforced slopes. The models in this series were built with a denser backfill sand but with the same reinforcement type as in the B-series.
- Stronger geotextile, S-series: Performed to investigate the effect of the reinforcement tensile strength on the performance of reinforced slopes. The models in this series were built using reinforcements with a higher tensile strength than in the B-series but with the same backfill density as in that series.

The history of centrifugal acceleration during centrifuge testing of one of the models is indicated in Figure 5. In this particular test, the acceleration was increased until sudden failure occurred after approximately 50 min of testing when the acceleration imparted to the model was 76.5 times the acceleration of gravity. Settlements at the crest of the slope, monitored by LVDTs, proved to be invaluable to accurately identify the moment of failure. Figure 6 shows the increasing settlements at the top of a reinforced slope model during centrifuge testing. The sudden increase in the monitored settlements indicates the moment of failure when the reinforced active wedge slid along the failure surface. Figure 7 shows a typical failure surface as developed in the centrifuge models. As can be seen, the failure surface is well defined and goes through the toe of the reinforced slope.

Following the test, each model was carefully disassembled in order to examine the tears in the geotextile layers. Figure 8 shows the geotextiles retrieved after centrifuge testing of a model reinforced with eighteen geotextile layers. The geotextile at the top left corner of the figure is the reinforcement layer retrieved from the base of the model. The geotextile at the bottom right corner is the reinforcement retrieved from the top of the model. All retrieved geotextiles show clear tears at the location of the failure surface. The pattern observed from the retrieved geotextiles shows that internal failure occurred when the tensile strength on the reinforcements was achieved. The geotextile layers located towards the base of the slope model also showed breakage of the geotextile overlaps, which clearly contributed to the stability of the slope. No evidence of pullout was observed, even on the short overlapping layers.

### **2.4 Effect of Backfill Shear Strength on the Experimental Results**

The criteria for characterizing reinforcements as extensible or inextensible has been established by comparing the horizontal strain in an element of reinforced backfill soil subjected to a given load, to the strain required to develop an active plastic state in an element of the same soil without reinforcement (Bonaparte and Schmertmann 1987). Accordingly, reinforcements have been typically classified as:

- extensible, if the tensile strain at failure in the reinforcement exceeds the horizontal extension required to develop an active plastic state in the soil; or as

## ZORNBERG • ADVANCES IN REINFORCED SOIL TECHNOLOGY

- inextensible, if the tensile strain at failure in the reinforcement is significantly less than the horizontal extension required to develop an active plastic state in the soil.

The geotextiles used to reinforce the centrifuge model slopes are extensible reinforcements. The effect of reinforcement spacing on the stability of the reinforced slope models, as indicated by the measured g-level at failure  $N_f$ , is shown in Figure 9. The number of reinforcement layers  $n$  in the figure includes the total number of model geotextiles intersected by the failure surface (i.e. primary reinforcements and overlaps intersected by the failure surface). The overlaps intersected by the failure surface developed tensile forces and eventually failed by breakage and not by pullout. The figure shows that a well-defined linear relationship can be established between the number of reinforcement layers and the g-level at failure. As the fitted lines for each test series passes through the origin, the results in each test series can be characterized by a single  $n/N_f$  ratio.

Models in the B- and D-series were reinforced using the same geotextile reinforcement, but using sand backfill placed at two different relative densities (55 and 75%). As mentioned, the Monterey sand at these two relative densities has the same soil residual friction angle ( $32.5^\circ$ ) but different peak friction angles ( $35^\circ$  and  $37.5^\circ$ ). As shown in Figure 9, models in the D-series failed at higher g-levels than models in the B-series built with the same reinforcement spacing and reinforcement type. Since the backfill soil in models from the D- and B-series have the same residual soil shear strength, the higher g-level at failure in the D-series models is due to the higher peak soil shear strength in this test series.

Analysis of the data presented in this figure emphasizes that the use of a single residual shear strength value, common to the two backfill materials used in the test series, can not explain the experimental results. Instead, the experimental results can be explained by acknowledging that the stability models constructed with the same reinforcement layout and the same sand backfill, but placed at different densities, is governed by different shear strength values. Indeed, limit equilibrium analyses (Zornberg et al. 1998b) indicated that the shear strength value that should be used in the analysis of these slope failures is the plain strain peak shear strength of the backfill.

The experimental results indicate that the stability of structures with extensible reinforcements is governed by the peak shear strength and not by the residual shear strength of the backfill soil. A plausible explanation of these experimental results is that, although the soil shear strength may have been fully mobilized along certain active failure planes within the reinforced soil mass, shear displacements have not taken place along these failure surfaces. That is, although the soil may have reached active state due to large horizontal strains because of the extensible nature of the reinforcements, large shear displacements (and drop from peak to residual soil shear strength) only take place along the failure surface during final sliding of the active reinforced wedge (Zornberg et al. 1998b).

An additional way of evaluating these experimental results is by using dimensionless coefficients, which have been used in order to develop design charts for geosynthetic-reinforced soil slopes (Schmertmann et al. 1987, Leshchinsky and Boedeker 1989, Jewell 1991). The validity of the proposed normalization can be investigated from the centrifuge results of this study. For a reinforced slope model that failed at an acceleration equal to  $N_f$  times the acceleration of gravity, a dimensionless coefficient  $K$  can be estimated as follows:

$$K = n T_{ult} \cdot \left( \frac{2}{\gamma H^2} \right) \cdot \frac{1}{N_f} \quad (1)$$

where  $n$  is the number of reinforcements,  $T_{ult}$  is the reinforcement tensile strength,  $H$  is the slope height,  $N_f$  is the g-level at failure from the centrifuge test, and  $\gamma$  is the sand unit weight. The value of  $n$  used in Equation 1 includes the number of overlaps that were intersected by the failure surface in the centrifuge slope models in addition to the number of primary reinforcement layers. The coefficient  $K$  is a function of the shear strength of the soil and of the slope inclination. [i.e.  $K = K(\phi, \beta)$ ]. All centrifuge slope models were built with the same slope inclination  $\beta$ . Consequently, validation of the suggested normalization requires that a single coefficient  $K(\phi, \beta)$  be obtained for all models built with the same backfill. If the soil shear strength governing failure of the models is the residual strength, a single coefficient  $K(\phi, \beta)$  should be obtained for all models. On the other hand, if the soil shear strength governing failure is the peak shear strength, a single coefficient should be obtained for those models built with sand placed at the same relative density.

Figure 10 shows the centrifuge results in terms of  $(n T_{ult}) (2 / \gamma H^2)$  versus the g-level at failure  $N_f$ . The results in the figure show that a linear relationship can be established for those models built with sand placed at the same relative density. As inferred from Equation 1, the slope of the fitted line corresponds to the dimensionless RTS coefficient  $K = K(\phi, \beta)$ . The results obtained using the centrifuge models from the B- and S-series, built using Monterey sand placed at 55% relative density, define a normalized coefficient  $K(\phi, \beta) = K_B = K_S = 0.084$ . Similarly, centrifuge results from the D-series models, built using Monterey sand at 75% relative density, define a normalized coefficient  $K(\phi, \beta) = K_D = 0.062$ . These results provide sound experimental evidence supporting the use of charts based on normalized coefficients for preliminary design of geosynthetic-reinforced slopes. If failure of reinforced soil slopes were governed by the residual soil shear strength, the results of all centrifuge tests should have defined a single line. However, as can be observed in the figure, different normalized coefficients are obtained for different soil densities. This confirms that the normalization should be based on the peak shear strength and not on the residual shear strength of the backfill material.

## 2.5 Final Remarks on Validation of Design Tools

The selection of the backfill shear strength properties in the design of geosynthetic-reinforced soil structures is an issue over which design guidelines disagree. The main debate has been over

whether the peak or the residual shear strength of the backfill material should be adopted for design. The use of residual shear strength values in the design of geosynthetic reinforced slopes while still using peak shear strength in the design of unreinforced embankments could lead to illogical comparisons of alternatives for embankment design. For example, an unreinforced slope that satisfies stability criteria based on a factor of safety calculated using peak strength, would become unacceptable if reinforced using inclusions of small (or negligible, for the purposes of this example) tensile strength because stability would be evaluated in this case using residual soil shear strength values. The main purpose of this investigation was to provide experimental evidence addressing this currently unsettled issue.

The experimental results presented herein indicate that the soil shear strength governing the stability of geosynthetic-reinforced soil slopes is the peak shear strength. A centrifuge experimental testing program was undertaken which indicated that reinforced slopes constructed with the same reinforcement layout and the same backfill sand, but using different sand densities failed at different centrifuge accelerations. That is, nominally identical models built with backfill material having the same residual shear strength but different peak shear strength did not have the same factor of safety. Since the residual shear strength of the sand backfill is independent of the relative density, these results indicate that the soil shear strength governing stability is the peak shear strength of the backfill material.

Several design guidance manuals have implicitly recommended the selection of the peak shear strength for the design of reinforced soil slopes. Considering the current debate over the selection of the soil shear strength in design and the experimental results presented herein, design manuals should explicitly endorse selection of peak shear strength values for the design of reinforced soil structures. This approach would not only be consistent with the observed experimental centrifuge results, but also with the US practice of using peak shear strength in the design of unreinforced slopes.

### **3 GEOSYNTHETIC-REINFORCED BRIDGE ABUTMENTS**

#### **3.1 Overview**

The technology of geosynthetic-reinforced soil (GRS) systems has been used extensively in transportation systems to support the self-weight of the backfill soil, roadway structures, and traffic loads. The increasing use and acceptance of soil reinforcement has been triggered by a number of factors, including cost savings, aesthetics, simple and fast construction techniques, good seismic performance, and the ability to tolerate large differential settlement without structural distress. A comparatively new use of this technology is the use of GRS systems as an integral structural component of bridge abutments and piers. Use of a reinforced soil system to directly support both the bridge (e.g. using a shallow foundation) and the approaching roadway structure has the potential of significantly reducing construction costs, decreasing construction

time, and smoothing the ride for vehicular traffic by eliminating the “bump at the bridge” caused by differential settlements between bridge foundations and approaching roadway structures.

The most prominent GRS abutment for bridge support in the U.S. is the recently-opened-to-traffic Founders/Meadows Parkway bridge, which crosses I-25 approximately 20 miles south of downtown Denver, Colorado (Figure 11). Designed and constructed by the Colorado Department of Transportation (CDOT), this is the first major bridge in the United States to be built on footings supported by a geosynthetic-reinforced system, eliminating the use of traditional deep foundations (piles) altogether. Phased construction of the almost 9-m high, horseshoe-shaped abutments, located on each side of the highway, began July 1998 and was completed twelve months later. Significant previous research by FHWA and CDOT on GRS bridge abutments, which has demonstrated their excellent performance and high load-carrying capacity, led to the construction of this unique structure.

The performance of bridge structures supported by GRS abutments has not been tested under actual service conditions to merit acceptance without reservation in highway construction. Consequently, the Founders/Meadows structure was considered experimental and comprehensive material testing, instrumentation, and monitoring programs were incorporated into the construction operations. Design procedures, material characterization programs, and monitoring results from the preliminary (Phase I) instrumentation program are discussed by Abu-Hejleh et al. (2000). Large-size direct shear and triaxial tests were conducted to determine representative shear strength properties and constitutive relations of the gravelly backfill used for construction. Three sections of the GRS system were instrumented to provide information on the structure movements, soil stresses, geogrid strains, and moisture content during construction and after opening the structure to traffic.

### **3.2 Past experiences in GRS bridge abutments**

Although the Founders/Meadows structure is a pioneer project in the U.S. involving permanent GRS bridge abutments for highway infrastructure, significant efforts have been undertaken in Japan, Europe and Australia regarding implementation of such systems in transportation projects. Japanese experience includes preloaded and prestressed bridge piers (Tatsuoka et al. 1997, Uchimura et al. 1998) and geosynthetic-reinforced wall systems with continuous rigid facing for railway infrastructure (Kanazawa et al. 1994, Tateyama et al. 1994). European experience includes vertically loaded, full-scale tests on geosynthetic reinforced walls constructed in France (Gotteland et al. 1997) and Germany (Brau and Floss 2000). Finally, Won et al. (1996) reported the use of three terraced geogrid-reinforced walls with segmental block facing to directly support end spans for a major bridge in Australia.

The experience in the U.S. regarding geosynthetic-reinforced bridge abutments for highway infrastructure includes full-scale demonstration tests conducted by the Federal Highway Administration (FHWA) (e.g. Adams 1997, 2000) and by CDOT (e.g. Ketchart and Wu 1997).

In the CDOT demonstration project, the GRS abutment was constructed with roadbase backfill reinforced with layers of a woven polypropylene geotextile placed at a spacing of 0.2 m. Dry-stacked hollow-cored concrete blocks were used as facing. A vertical surcharge of 232 kPa was applied to the 7.6 m high abutment structure. The measured immediate maximum vertical and lateral displacements were 27.1 mm and 14.3 mm, respectively. The maximum vertical and lateral creep displacements after a sustained vertical surcharge pressure of 232 kPa, applied during 70 days, were 18.3 mm and 14.3 mm, respectively. The excellent performance and high loading capacity demonstrated by these geosynthetic-reinforced soil abutments with segmental block facing convinced CDOT design engineers to select GRS walls to support the bridge abutment at the Founders/Meadows structure.

### 3.3 Description of the GRS bridge abutment

The Founders/Meadows bridge is located 20 miles south of Denver, Colorado, near Castle Rock. The bridge carries Colorado State Highway 86, Founders/Meadows Parkway, over U.S. Interstate 25. This structure, completed by CDOT in July of 1999, replaced a deteriorated two-span bridge structure. In this project, both the bridge and the approaching roadway structures are supported by a system of geosynthetic-reinforced segmental retaining walls. Figure 12 shows a picture of one of the segmental retaining wall systems, located at the east side of the bridge. This figure shows the bridge superstructure supported by the “front MSE wall,” which extends around a 90-degree curve into a “lower MSE wall” supporting the “wing wall” and a second tier, “upper MSE wall”.

Each span of the new bridge is 34.5 m long and 34.5 m wide, with 20 side-by-side prestressed box girders. The new bridge is 13 m longer and 25 m wider than the previous structure, accommodating six traffic lanes and sidewalks on both sides of the bridge. A typical monitored cross-section through the “front MSE wall” and “abutment wall” transmits the load through abutment walls to a shallow strip footing placed directly on the top of a geogrid-reinforced segmental retaining wall. The centerline of the bridge abutment wall and edge of the foundation are located 3.1 m and 1.35 m, respectively, from the facing of the front MSE wall. A short reinforced concrete abutment wall and two wing walls, resting on the spread foundation, confine the reinforced backfill soil behind the bridge abutment and support the bridge approach slab. The bridge is supported by central pier columns along the middle of the structure, which in turn are supported by a spread footing founded on bedrock at the median of U.S. Interstate 25.

When compared to typical systems involving the use of deep foundations to support bridge structures, the use of geosynthetic-reinforced systems to support both the bridge and the approaching roadway structures has the potential to alleviate the “bump at the bridge” problem caused by differential settlements between the bridge abutment and approaching roadway. In addition, this approach also allows for construction in stages and comparatively smaller construction working areas. Several of the common causes for development of bridge bumps were addressed in the design of the Founders/Meadows structure. The main cause of uneven

settlements in typical systems is the use of different foundation types. That is, while the approaching roadway structure is typically constructed on compacted backfill soil (reinforced or not), the bridge abutment is typically supported on stronger soils by deep foundations. The roadway approach embankment and the bridge footing were integrated at the Founders/Meadows structure with an extended reinforced soil zone in order to minimize uneven settlements between the bridge abutment and approaching roadway. A second cause of differential settlements can be attributed to erosion of the fill material around the abutment wall induced by surface water runoff. Several measures were implemented in this project to prevent that surface water, as well as groundwater, reach the reinforced soil mass and the bedrock at the base of the fill (e.g. placement of impervious membranes with collector pipes). Finally, a third potential cause of differential settlements is the thermally induced movements, i.e., expansion and contraction of bridge girders strongly attached to the abutment wall (integral abutment). A compressible 75 mm low-density expanded polystyrene sheet was placed between the reinforced backfill and the abutment walls. It was expected that this system would accommodate the thermally induced movements of the bridge superstructure without affecting the retained backfill.

The backfill soil used in this project includes fractions of gravel (35%), sand (54.4%), and fine-grained soil (10.6%). The liquid limit and plasticity index for the fine fraction of the backfill are 25% and 4 %, respectively. The backfill soil classifies as SW-SM per ASTM 2487, and as A-1-B (0) per AASHTO M 145. The backfill met the construction requirements for CDOT Class 1 backfill. A friction angle of 34° and zero cohesion were assumed in the design of the GRS walls. To evaluate the suitability of these design parameters, conventional direct shear tests and large size direct shear and triaxial tests were conducted. In the conventional tests, the 35% gravel portion was removed from the specimens, but in the large-size triaxial and direct shear tests, the backfill soil specimens included the gravel portion. The results of conventional direct shear tests and large size direct shear and triaxial tests indicate that assuming zero cohesion in the design procedure and removing the gravel portion from the test specimens lead to significant underestimation of the actual shear strength of the backfill.

The geogrid reinforcements used in this project were manufactured by the Tensar Corporation. Three types of geogrid reinforcements were used: UX 6 below the footing, and UX 3 and UX 2 behind the abutment wall. The long-term-design-strength (LTDS) of these reinforcements is 27 kN/m, 11 kN/m, and 6.8 kN/m, respectively. CDOT specifications imposed a global reduction factor of 5.82 to determine the long-term design strength (LTDS) of the geogrid reinforcements from their ultimate strength. This global reduction factor accounts for reinforcement tensile strength losses over the design life period due to creep, durability, and installation damage. It also includes a factor of safety to account for uncertainties.

### **3.4 Performance**

The instrumentation program was conducted in two phases (Phases I and II), which correspond, respectively to the construction of two phases of the GRS bridge abutment structure. A pilot instrumentation plan was conducted during construction of the Phase I structure in order to

obtain information that will tailor the design of a more comprehensive monitoring program to be implemented during Phase II. The Phase I instrumentation program included survey targets, pressure cells, jointmeters, and inclinometer. The more comprehensive Phase II instrumentation program included monitoring using survey targets, digital road profiler, pressure cells, strain gauges, moisture gauges, and temperature gauges. A view of the instrumentation plan for Phase II is shown in **Figure 13**. The figure shows the four critical locations that were instrumented in Phase II:

- (i) Location A, close to the facing. Data collected at this location is particularly useful for guiding the structural design of the facing and of the connection between facing and reinforcements.
- (ii) Locations B and C along the center and interior edge of the abutment foundation. Information collected at these locations is relevant for the design of the reinforcement elements.
- (iii) Location D, behind the bridge foundation, and horizontal plane at the base of the fill. Data measured at these locations is useful to estimate the external forces acting behind and below the reinforced soil mass.

A comprehensive discussion of the instrumentation results, the collection and analysis of which is under progress, is beyond the scope of this paper. Results of the preliminary Phase I instrumentation program have been reported by Abu-Hejleh et al. (2000). Some of the relevant findings obtained based on the information collected so far are the following:

- The measured response from both the pressure cells and strain gauges correlates well with the applied loads during the construction stages.
- The maximum geogrid strains experienced during construction are comparatively very small (approximately 0.45 %).
- Horizontal earth pressures collected at the facing and of the reinforcement maximum tensile strains are well below design values.
- Most of the straining of the geogrid reinforcements occurred during construction of the wall and not during placement of the bridge surcharge load. This can be explained by the effect of compaction operations and presence of slacks in the geogrid reinforcements. Strain gauge monitoring results collected so far suggest that approximately 50% of the total recorded strains occurred during placement and compaction of a few lifts of soil above the geogrid layers (e.g. approximately 2 m of soil or 40 kPa). The maximum measured front wall outward displacement induced by wall construction (before placement of the bridge superstructure) was 12 mm, which corresponds to 0.20 % of the wall height.
- The maximum outward displacement induced by placement of the bridge superstructure was additional 10 mm, which corresponds to 0.17% of the wall height. The maximum settlement of the bridge footing due to placement of the bridge superstructure was 13 mm.

## ZORNBERG • ADVANCES IN REINFORCED SOIL TECHNOLOGY

- The maximum outward displacements induced after opening the structure to traffic and until June 2000 (18 months) was 13 mm. These movements correspond to 0.22 % of the wall height. The measured settlement of the leveling pad supporting the front wall facing was approximately 5 mm. However, it is important to emphasize that these movements took place only during the initial 12 months of service (until January 2000). Lateral and vertical movements have been negligible from January to June 2000.
- Elevation profiling and surveying results show no signs of development of the “bump at the bridge” problem.

Overall, the performance of the Founders/Meadows bridge structure, based on the monitored behavior recorded so far, showed excellent short- and long-term performance. Specifically, the monitored movements were significantly smaller than those expected in design or allowed by performance requirements, there were no signs for development of the “bump at the bridge” problem or any structural damage, and post-construction movements became negligible after an in-service period of 1 year.

## 4 ADVANCES IN FIBER-REINFORCED SOIL DESIGN

### 4.1 Overview

Fiber reinforcement has become a promising solution to the stabilization of thin soil veneers and localized repair of failed slopes. Randomly distributed fibers can maintain strength isotropy and avoid the existence of the potential planes of weakness that can develop parallel to continuous planar reinforcement elements. The design of fiber-reinforced soil slopes has typically been performed using composite approaches, where the fiber-reinforced soil is considered a single homogenized material. Accordingly, fiber-reinforced soil design has required non-conventional laboratory testing of composite fiber-reinforced soil specimens which has discouraged implementation of fiber-reinforcement in engineering practice.

Several composite models have been proposed to explain the behavior of randomly distributed fibers within a soil mass (Maher and Gray, 1990, Michalowski and Zhao, 1996, Ranjan et al., 1996). The mechanistic models proposed by Gray and Ohashi (1983) and Maher and Gray (1990) quantify the “equivalent shear strength” of the fiber-reinforced composite as a function of the thickness of the shear band that develops during failure. Information needed to characterize shear band development for these models is, however, difficult to quantify (Shewbridge and Sitar, 1990). Common findings from the various testing programs implemented to investigate composite models include: (i) randomly distributed fibers provide strength isotropy in a soil composite; (ii) fiber inclusions increase the “equivalent” shear strength within a reinforced soil mass; and (iii) the “equivalent” strength typically shows a bilinear behavior, which was experimentally observed by testing of comparatively weak fibers under a wide range of confining stresses.

A discrete approach for the design of fiber-reinforced soil slopes was recently proposed to characterize the contribution of randomly distributed fibers to stability (Zornberg, 2002). In this approach, fiber-reinforced soil is characterized as a two-component (soil and fibers) material. Fibers are treated as discrete elements that contribute to stability by mobilizing tensile stresses along the shear plane. Consequently, independent testing of soil specimens and of fiber specimens, but not of fiber-reinforced soil specimens, can be used to characterize fiber-reinforced soil performance.

This paper initially reviews the main concepts of the discrete approach and subsequently validates the framework for design purposes.

#### 4.2 Discrete frame work for fiber reinforcement

The volumetric fiber content,  $\chi$ , used in the proposed discrete framework is defined as:

$$\chi = \frac{V_f}{V} \quad (1)$$

where  $V_f$  is the volume of fibers and  $V$  is the control volume of fiber-reinforced soil.

The gravimetric fiber content,  $\chi_w$ , typically used in construction specifications, is defined as:

$$\chi_w = \frac{W_f}{W_s} \quad (2)$$

where  $W_f$  is the weight of fibers and  $W_s$  is the dry weight of soil.

The dry unit weight of the fiber-reinforced soil composite,  $\gamma_d$ , is defined as:

$$\gamma_d = \frac{W_f + W_s}{V} \quad (3)$$

The contribution of fibers to stability leads to an increased shear strength of the “homogenized” composite reinforced mass. However, the reinforcing fibers actually work in tension and not in shear. A major objective of the discrete framework is to explicitly quantify the fiber-induced distributed tension,  $t$ , which is the tensile force per unit area induced in a soil mass by randomly distributed fibers.

Specifically, the magnitude of the fiber-induced distributed tension is defined as a function of properties of the individual fibers. In this way, as in analysis involving planar reinforcements, limit equilibrium analysis of fiber-reinforced soil can explicitly account for tensile forces.

The interface shear strength of individual fibers can be expressed as:

$$f_f = c_{i,c} \cdot c + c_{i,\phi} \cdot \tan \phi \cdot \sigma_{n,ave} \quad (4)$$

where  $c$  and  $\phi$  are the cohesive and frictional components of the soil shear strength and  $\sigma_{n,ave}$  is the average normal stress acting on the fibers. The interaction coefficients,  $c_{i,c}$  and  $c_{i,\phi}$ , commonly used in soil reinforcement literature for continuous planar reinforcement, is adopted herein to relate the interface shear strength to the shear strength of the soil. The interaction coefficients are defined as:

$$c_{i,c} = \frac{a}{c} \quad (5)$$

$$c_{i,\phi} = \frac{\tan \delta}{\tan \phi} \quad (6)$$

where  $a$  is the adhesive component of the interface shear strength between soil and the polymeric fiber,  $\tan \delta$  is the skin-frictional component.

The pullout resistance of a fiber of length  $l_f$  should be estimated over the shortest side of the two portions of a fiber intercepted by the failure plane. The length of the shortest portion of a fiber intercepted by the failure plane varies from zero to  $l_f/2$ . Statistically, the average embedment length of randomly distributed fibers,  $l_{e,ave}$ , can be analytically defined by:

$$l_{e,ave} = \frac{l_f}{4} \quad (7)$$

where  $l_f$  is total length of the fibers.

The average pullout resistance can be quantified along the average embedment length,  $l_{e,ave}$ , of all individual fibers crossing a soil control surface  $A$ . The ratio between the total cross sectional area of the fibers  $A_f$  and the control surface  $A$  is assumed to be defined by the volumetric fiber content  $\chi$ . That is:

$$\chi = \frac{A_f}{A}$$

When failure is governed by the pullout of the fibers, the fiber-induced distributed tension,  $t_p$ , is defined as the average of the tensile forces inside the fibers over the control area  $A$ . Consequently,  $t_p$  can be estimated as:

$$t_p = \chi \cdot \eta \cdot (c_{i,c} \cdot c + c_{i,\phi} \cdot \tan \phi \cdot \sigma_{n,ave}) \quad (9)$$

where  $\eta$  is the aspect ratio defined as:

$$\eta = \frac{l_f}{d_f} \quad (10)$$

where  $d_f$  is the equivalent diameter of the fiber.

When failure is governed by the yielding of the fibers, the distributed tension,  $t_t$ , is determined from the tensile strength of the fiber:

$$t_t = \chi \cdot \sigma_{f,ult}$$

where  $\sigma_{f,ult}$  is the ultimate tensile strength of the individual fibers.

The fiber-induced distributed tension  $t$  to be used in the discrete approach to account for the tensile contribution of the fibers in limit equilibrium analysis is:

$$t = \min(t_p, t_t) \quad (12)$$

The critical normal stress,  $\sigma_{n,crit}$ , which defines the change in the governing failure mode, is the normal stress at which failure occurs simultaneously by pullout and tensile breakage of the fibers. That is, the following condition holds at the critical normal stress:

$$t_t = t_p \quad (13)$$

An analytical expression for the critical normal stress can be obtained as follows:

$$\sigma_{n,crut} = \frac{\sigma_{f,ult} - \eta \cdot c_{i,c} \cdot c}{\eta \cdot c_{i,\phi} \cdot \tan \phi} \quad (14)$$

As in analyses involving planar inclusions, the orientation of the fiber-induced distributed tension should also be identified or assumed. Specifically, the fiber-induced distributed tension can be assumed to act: a) along the failure surface so that the discrete fiber-induced tensile contribution can be directly “added” to the shear strength contribution of the soil in a limit equilibrium analysis; b) horizontally, which would be consistent with design assumptions for reinforced soil structures using planar reinforcements; and c) in a direction somewhere between the initial fiber orientation (which is random) and the orientation of the failure plane.

This equivalent shear strength of fiber-reinforced specimens can be defined as a function of the fiber-induced distributed tension  $t$ , and the shear strength of the unreinforced soil,  $S$ :

$$S_{eq} = S + \alpha \cdot t = c + \sigma_n \tan \phi + \alpha \cdot t \quad (15)$$

where  $\alpha$  is an empirical coefficient that accounts for the orientation of fiber and the efficiency of the mixing of fibers.  $\alpha$  is equal to 1, if the fibers are randomly distributed and working with 100% efficiency, otherwise  $\alpha$  should be smaller than 1.

Depending on whether the mode of failure is fiber pullout or yielding, the equivalent shear strength can be derived by combining (9) or (11) with (15). It should be noted that the average normal stress acting on the fibers,  $\sigma_{n,ave}$ , does not necessarily equal the normal stress on the shear plane  $\sigma_n$ . For randomly distributed fibers,  $\sigma_{n,ave}$  could be represented by the octahedral stress component. However, a sensitivity evaluation undertaken using typical ranges of shear strength parameters show that  $\sigma_{n,ave}$  can be approximated by  $\sigma_n$  without introducing significant error.

Accordingly, the following expressions can be used to define the equivalent shear strength when failure is governed by fiber pullout:

$$S_{eq,p} = c_{eq,p} + (\tan \phi)_{eq,p} \cdot \sigma_n \quad (16)$$

$$c_{eq,p} = (1 + \alpha \cdot \eta \cdot \chi \cdot c_{i,c}) \cdot c \quad (17)$$

$$(\tan \phi)_{eq,p} = (1 + \alpha \cdot \eta \cdot \chi \cdot c_{i,\phi}) \cdot \tan \phi \quad (18)$$

Equivalently, the following expressions can be obtained to define the equivalent shear strength when failure is governed by tensile breakage of the fibers:

$$S_{eq,t} = c_{eq,t} + (\tan \phi)_{eq,t} \cdot \sigma_n \quad (19)$$

$$c_{eq,t} = c + \alpha \cdot \chi \cdot \sigma_{f,ult} \quad (20)$$

$$(\tan \phi)_{eq,t} = \tan \phi \quad (21)$$

The above expressions yield a bilinear shear strength envelope, which is shown in Figure 14.

## 4.2 Experimental validation

A triaxial compression testing program on fiber-reinforced soil was implemented to validate the proposed discrete framework. Both cohesive and granular soils were used in the testing program, and the soil properties were summarized in Table 2.

The tests were conducted using commercially available polypropylene fibers, and the properties of fibers were summarized in Table 3. A series of tensile test were performed in general accordance with ASTM D2256-97 to evaluate the ultimate tensile strength of fibers. The average tensile strength of the fibers was approximately 425,000 kPa.

The triaxial testing program involved consolidated drained (CD) tests for SP soils and consolidated undrained (CU) tests for CL soils. The specimens have a diameter of 71 mm and a minimum length-to-diameter ratio of 2. The CU tests were performed in general accordance with ASTM D4767, and the specimens were back pressure saturated and the pore water pressure was measured. The unreinforced tests of SP soil yielded an effective shear strength envelope defined by cohesion of 6.1 kPa and friction angle of 34.3°, while the cohesion and friction angle of CL soil were 12.0 kPa and 31.0° respectively.

The governing failure mode for the polymeric fibers used in this investigation is pullout because of the comparatively high tensile strength and short length of the fibers. Accordingly, the triaxial testing program conducted in this study focuses only on the first portion of the bilinear strength envelope shown in Figure 1.

Figure 15 shows the stress-strain behavior of SP soil specimens reinforced with 360 denier fibers, and placed at gravimetric fiber contents of 0, 0.2 and 0.4 %. Specimens were tested under confining pressure of 70 kPa. The peak deviator stress increases approximately linearly with increasing fiber content, which is consistent with the discrete framework (see equation (9)). The post-peak shear strength loss is smaller in the reinforced specimens than in the unreinforced specimens. However, the initial portions of the stress-strain curves of the reinforced and unreinforced specimens are approximately similar. Accordingly, the soil appears to take most of the applied load at small strain levels, while the load resisted by the fibers is more substantial at higher strain level. The larger strain corresponding to the peak deviator stress displayed by the fiber-reinforced specimens suggests that fibers increase the ductility of the reinforced soil specimen. These findings are confirmed in Figure 3, which shows the test results obtained under higher confining stress (140 kPa).

The effect of fiber length on the stress-strain behavior is shown in Figure 4. The specimens were prepared using fibers with a different fiber type (1000 denier) than that used in the tests shown in Figures 16 and 17. The specimens were prepared using the same gravimetric fiber content, but with varying fiber length. The specimens reinforced with longer (50 mm) fibers displayed higher shear strength. The peak deviator stress increases linearly with increasing aspect ratio, which is also consistent with the trend indicated by equation (9). The strain corresponding to the peak strength increases with increasing fiber length. When the governing failure mode is pullout, the fiber-induced distributed tension reaches its peak when the pullout resistance is fully mobilized. For longer fibers, it usually requires a larger interface shear deformation to fully mobilize the interface strength. Consequently, the macroscopic axial strain at peak stress should be larger for specimen reinforced with longer fibers. Figure 18 shows a similar trend for the case of tests conducted under higher confining pressures.

Figure 19 compares the stress-strain behavior of both unreinforced and fiber-reinforced specimen using soil 2. The reinforced specimen were prepared at  $\chi_w=0.2\%$ , using 2-inch long 2610 denier fibers. Both specimens were compacted at optimum moisture content to 90% of the maximum dry density achieved in the standard Proctor test as specified in ASTM D 698, and tested under confining pressure  $\sigma_3=98$  kPa. Due to the undrained test condition, the effective confining stress changes with the excess pore water pressure induced in the process of shearing. The peak shear strength was selected in terms of the maximum value of  $(\sigma_1'/\sigma_3')$ . The increment of deviator stress due to fiber addition is not as obvious as in the case of SP sand. However, the pore water pressure generated during shearing is larger for reinforced specimen than for unreinforced specimen (see Figure 20). Consequently the effective confining stress inside the reinforced specimen is smaller than that inside the unreinforced specimen. The fiber-reinforced specimen achieved equal or higher peak deviator stress than the unreinforced specimen under a lower effective confining stress. This shows that the addition of fibers increases the shear strength of the reinforced specimen. Since positive water pressure is associated with the tendency of volume shrinkage, this observation shows that fiber reinforcement restrains the dilatancy of the reinforced soil. Other researchers (Michalowski and Cermak, 2003, Consoli et al., 1998) reported that fiber-reinforced specimens displayed smaller volume dilatation than unreinforced specimen in consolidated drained (CD) test. This observation confirms their findings in a different test condition.

Similar observation can be made from Figures 8 and 9, which shows the stress-strain behavior and the pore water pressure evolution obtained using 25-mm fibers placed at 0.2% and 0.4% gravimetric fiber contents. As the fiber content increases, the pore water pressure generated during undrained shearing also increases.

Equations (16) through (18) were used to predict the equivalent shear strength for fiber-reinforced specimens. Interaction coefficients ( $c_{i,c}$  and  $c_{i,\phi}$ ) of 0.8 are assumed in the analyses conducted in this study. The interface shear strength obtained from pullout test results conducted on woven geotextiles was considered representative of the interface shear strength on individual

fibers. For practical purposes, interaction coefficients can be selected from values reported in the literature for continuous planar reinforcements. This is because pullout tests conducted using a variety of soils and planar geosynthetics have been reported to render interaction coefficient values falling within a narrow range (Koutsourais et al., 1998, Michalowski and Cermak, 2003).  $\alpha$  is assumed to be 1.0 for randomly distributed fibers. Table 4 summarized the values of parameters used in the analyses.

The effect of fiber content on shear strength is shown in Figure 23, which compares the experimental data and predicted shear strength envelopes obtained from Soil 1 using 25 mm fibers with linear density of 360 denier placed at fiber contents of 0.0%, 0.2%, and 0.4%. The experimental results show a clear increase in equivalent shear strength with increasing fiber content. No major influence of fibrillation is perceived in the results of the testing program. The shear strength envelope for the unreinforced specimens was defined by fitting the experimental data. However, the shear strength envelopes shown in the figure for the reinforced specimens were predicted analytically using the proposed discrete framework. A very good agreement is observed between experimental data points and predicted shear strength envelopes. As predicted by the discrete framework, the distributed fiber-induced tension increases linearly with the volumetric fiber content. Similar observation can be made in Figure 24, which shows the results obtained from Soil 2 using 50- mm-long fibers with linear density of 2610 denier.

The effect of fiber aspect ratio on shear strength is shown in Figure 25, which compares the experimental and predicted shear strength envelopes of specimens of Soil 1 placed at  $\chi_w=0.2\%$ , with 25 and 50 mm-long fibers. As predicted by the discrete framework, increasing the fiber length increases the pullout resistance of individual fibers, and results in a higher fiber-induced distributed tension. Consequently, for the same fiber content, specimens reinforced with longer fibers will have higher equivalent shear strength. This trend agrees well with the experimental data. Similar observation can be made from Figure 26, which shows the results obtained from Soil 2 using 25 mm and 50 mm-long fibers and placed at  $\chi_w=0.4\%$ .

Additional insight into the validity of the proposed discrete approach can be obtained by comparing the results obtained for specimens reinforced with 50 mm-long fibers placed at a fiber content of 0.2% with those obtained for specimens reinforced with 25 mm-long fibers placed at a fiber content of 0.4%. That is specimens with a constant value of  $(\chi_w \cdot \eta)$ . As inferred from inspection of equation (9) the fiber-induced distributed tension is directly proportional to both the fiber content and the fiber aspect ratio. Consequently, the predicted equivalent shear strength parameters for the above combinations of fiber length and fiber content are the same. Figures 27 and 28 combine these experimental results.

The good agreement between experimental results and predicted values provides additional evidence of the suitability of the proposed discrete approach. From the practical standpoint, it should be noted that using 50 mm-long fibers placed at a fiber content of 0.2% corresponds to half the reinforcement material than using 25 mm-long fibers placed at a fiber content of 0.4%.

That is, for the same target equivalent shear strength the first combination leads to half the material costs than the second one. It is anticipated, though, that difficulty in achieving good fiber mixing may compromise the validity of the relationships developed herein for comparatively high aspect ratios (i.e. comparatively long fibers) and for comparatively high fiber contents. The fiber content or fiber length at which the validity of these relationships is compromised should be further evaluated. Nonetheless, good mixing was achieved for the fiber contents and fiber lengths considered in this investigation, which were selected based on values typically used in geotechnical projects.

Figure 29 shows the stress-strain behavior of specimen reinforced with 50 mm fibers placed at  $\chi_w = 0.2\%$  and 25 mm fibers placed at  $\chi_w = 0.4\%$ . While the discrete approach was developed only to predict the shear strength response, the results in the figure show that fiber-reinforced specimens prepared using a constant value display similar stress-strain behavior. This similar response is observed for both fibrillated and tape fibers, suggesting that the fibrillation procedure does not have a significant impact on the mechanical response of fiber-reinforced soil. The experimental results suggest that the proportionality of shear strength with the fiber content and fiber aspect ratio predicted by the discrete framework can be extrapolated to the entire stress-strain response of fiber-reinforced specimens.

#### 4.3 Remarks on Fiber Reinforced Soil

The discrete approach for fiber-reinforced soil was validated in this investigation using experimental data from a triaxial testing of both sand and clay. The effect of fiber reinforcement on stress-strain behavior and shear strength was investigated and compared with the analytical results of the discrete approach. The main conclusions drawn from this investigation are:

- The addition of fibers can significantly increase the peak shear strength and limit the post peak strength loss of both cohesive and granular soil. An increase in fiber content leads to increasing strain at failure and, consequently, to a more ductile behavior.
- The fiber reinforcement tends to restrain the volume dilation of the soil in drained condition, or equivalently, increase the positive water pressure in undrained condition.
- The peak shear strength increases with increasing aspect ratio. The strain at peak deviator stress increases with increasing fiber aspect ratio.
- As predicted by the discrete framework, the experimental results confirmed that the fiber-induced distributed tension increases linearly with fiber content and fiber aspect ratio when failure is characterized by pullout of individual fibers.
- Experimental results conducted using specimens with a constant ( $\chi_w \cdot \eta$ ) value show not only the same shear strength but also display a similar stress-strain behavior.

## ZORNBERG • ADVANCES IN REINFORCED SOIL TECHNOLOGY

- If good mixing can be achieved, fibers with comparatively high aspect ratio can lead to lower fiber contents while reaching the same target equivalent shear strength, resulting in savings of reinforcement material.
- Overall, for both sand and clay specimens, the discrete approach was shown to predict accurately the shear strength obtained experimentally using specimens reinforced with polymeric fibers tested under confining stresses typical of slope stabilization projects.

## REFERENCES

- AASHTO, 1996, *Standard specifications for highway bridges*. American Association of State Highway and Transportation Officials, Washington, D.C., USA.
- Abu-Hejleh, N. Wang, T., and Zornberg, J. G. (2000). "Performance of geosynthetic-reinforced walls supporting bridge and approaching roadway structures." *Advances in Transportation and Geoenvironmental Systems using Geosynthetics*, ASCE Geotechnical Special Publication No. 103, Zornberg, J.G. and Christopher, B.R. (Eds.), pp. 218-243.
- Adams, M. (1997). "Performance of a prestained geosynthetic reinforced soil bridge pier." *Int. Symp. On Mechanically Stabilized Backfill*, T.H. Wu, editor, A. A. Balkema, Denver, USA, 35-53.
- Adams, M. (2000). "Reinforced soil technology at FHWA – Making old technology new." *Geotechnical Fabrics Report*, August 2000, pp. 34-37.
- Bolton, M., 1986, "The Strength and Dilatancy of Sands." *Géotechnique*, Vol. 36, No. 1, pp. 65-78.
- Bonaparte, R. and Schmertmann, G.R., 1987, "Reinforcement Extensibility in Reinforced Soil Wall Design." *The Application of Polymeric Reinforcement in Soil Retaining Structures*, pp. 409-457.
- Brau, G. and Floss, R. (2000). "Geotextile structures used for the reconstruction of the motorway Munich-Salzburg." *Proceedings of Second European Geosynthetics Conference*, Bologna, Italy, Vol. 1, pp. 373-377.
- British Standards Institution, 1995, BS 8006:1995, *Code of Practice for Strengthened/Reinforced Soil and Other Fills*, P.162, BSI, London.
- Canadian Geotechnical Society, 1992, *Canadian Foundation Engineering Manual*. 3rd Edition.
- Christopher, B., Bonczkiewicz, C., and Holtz, R., 1992, "Design, Construction and Monitoring of Full Scale Test of Reinforced Soil Walls and Slopes." *Recent Case Histories of Permanent Geosynthetic-Reinforced Soil Retaining Walls*, Tokyo, Japan: A.A. Balkema, pp. 45-60.
- Consoli N.C., Prietto P.D.M., Ulbrich L.A. 1998, "Influence of Fiber and Cement Addition on Behavior of Sandy Soil", *ASCE J. of Geotech. and Geoenviron. Engrg.*, 124(12): pp. 1211-1214
- EBGEO, 1997, *Empfehlungen für Bewehrungen aus Geokunststoffen*, Ernst & Sohn Verlag.

## ZORNBERG • ADVANCES IN REINFORCED SOIL TECHNOLOGY

- Elias, V., Christopher, B.R., Berg, R.R., 2001, *Mechanically Stabilized Earth Walls and Reinforced Soil Slopes*. Publication Number FHWA NH-00-043, March 2001, NHI-FHWA.
- GCO, 1989, *Model Specification for Reinforced Fill Structures*, Geospec 2, Geotechnical Engineering Office, Hong Kong.
- GEO, 1993, *A Partial Factor Method for Reinforced Fill Slope Design*, GEO Report No. 34, Geotechnical Engineering Office, Hong Kong.
- GeoRio, 1999, *Technical Manual for Slope Stabilization*. (in Portuguese). Foundation for Slope Stability Control in the City of Rio de Janeiro, Volumes 1-4, Rio de Janeiro, Brazil, 682 p.
- Gotteland, Ph., Gourc, J.P., and Villard, P. (1997). "Geosynthetic reinforced structures as bridge abutment: Full Scale experimentation and comparison with modelisations." *Int. Symp. On Mechanically Stabilized Backfill*, T.H. Wu, editor, A. A. Balkema, Denver, USA, 25-34.
- Gray, D.H. and Ohashi, H. (1983). "Mechanics of Fiber-reinforcement in Sand", *ASCE J. Geotech. Engrg.* 109(3): pp. 335-353.
- Gourc, J.P., Arab, R., and Giraud, H., 2001, "Calibration and Validation of Design Methods for Geosynthetic-Reinforced Retaining Structures using Partial Factors," *Geosynthetics International*, Vol.8, No. 2, pp. 163-191.
- Jewell, R. A., 1991, "Application of revised design charts for steep reinforced slopes." *Geotextiles and Geomembranes*, Vol. 10, pp. 203-233.
- Ketchart, K. and Wu, J.T.H. (1997). "Performance of geosynthetic-reinforced soil bridge pier and abutment, Denver, Colorado, USA." *International Symposium on Mechanically Stabilized Backfill*, T.H. Wu (Ed.), Balkema, pp. 101-116.
- Koutsourais, M., Sandri, D., and Swan, R. (1998). "Soil Interaction Characteristics of Geotextiles and Geogrids". *Proc. 6th Int. Conf. Geosynthetics*, Atlanta, Georgia, March 1998, pp. 739-744.
- Leshchinsky, D., 2000, Discussion on "Performance of geosynthetic reinforced slopes at failure." By Zornberg, Sitar, and Mitchell, *Journal of Geotechnical and Geoenvironmental Engineering*, ASCE, Vol. 126, No. 3, pp. 281-283.
- Leshchinsky, D., 2001, "Design Dilemma: Use peak or residual strength of soil." *Geotextiles and Geomembranes*, Vol. 19, pp. 111-125.
- Leshchinsky, D. and Boedeker, R.H., 1989, "Geosynthetic Reinforced Soil Structures." *Journal of Geotechnical Engineering*, ASCE, Vol. 115, No. 10, pp. 1459-1478.
- Li, X.S., Chan, C.K., and Shen, C.K., 1988, "An Automated Triaxial Testing System." *Advanced Triaxial Testing of Soil and Rock*, ASTM STP 977, pp. 95-106.
- Maher, M.H. and Gray, D.H. (1990). "Static Response of Sand Reinforced With Randomly Distributed Fibers", *ASCE J. Geotech. Engrg.* 116(11): pp. 1661-1677.
- McGown, A., Murray, R.T., and Jewell, R.A., 1989, "State-of-the-art report on reinforced soil." *Proc., 12th Int. Conference Soil Mechanics and Foundation Engineering*, Rio de Janeiro, Vol. 4.
- Michalowski R.L., Cermak, J. (2003), "Triaxial compression of sand reinforced with fibers", *ASCE J. of Geotech. and Geoenviron. Engrg.*, 129(2): pp. 125-136
- Michalowski, R.L. and Zhao, A. (1996). "Failure of Fiber-Reinforced Granular Soils". *ASCE J. Geotech. Engrg.* 122(3): pp. 226-234.

## ZORNBERG • ADVANCES IN REINFORCED SOIL TECHNOLOGY

- National Concrete Masonry Association, 1997, *Design Manual for Segmental Retaining Walls*, Second edition, Second printing, J. Collin (Editor), Herndon, Virginia.
- National Concrete Masonry Association, 1998, *Segmental Retaining Walls – Seismic Design Manual*, 1st Edition, Bathurst (Editor), Herndon, Virginia.
- National Road Administration Publication 1992:10, 1992, *Soil reinforcement – Design tensile strength for synthetic materials* (In Swedish).
- Public Works Research Center, 2000, *Design Manual for Geotextile Reinforced Soil* (in Japanese).
- QMRD, 1997, *Reinforced Soil Structures*, Specification MRS11.06, Main Roads Department, Queensland, Australia.
- Ranjan, G., Vassan, R.M. and Charan, H.D. (1996). “Probabilistic Analysis of Randomly Distributed Fiber-Reinforced Soil”, *ASCE J. Geotech. Engrg.* 120(6): pp. 419-426.
- Riemer, M.F., 1992, *The Effects of Testing Conditions on the Constitutive Behavior of Loose, Saturated Sand under Monotonic Loading*, Ph.D. Dissertation, Dept. of Civil Engineering, Univ. of California, Berkeley.
- RTA, 1997, *Design of Reinforced Soil Walls*, QA Specification R57, Roads and Traffic Authority, New South Wales, Australia.
- Schmertmann, G. R., Chouery-Curtis, V.E., Johnson, R.D., and Bonaparte, R., 1987, “Design Charts for Geogrid-Reinforced Soil Slopes.” *Proc., Geosynthetics’87 Conference*, New Orleans, pp. 108-120.
- Shewbridge, S.E. and Sitar, N. (1990). “Deformation Based Model for Reinforced Sand”, *ASCE J. Geotechnical Engineering* 116(7): pp. 1153-1170.
- Tatsuoka, F., Uchimura, T., and Tateyama, M. (1997) “Preloaded and prestressed reinforced soil.” *Soils and Foundations*, Vol. 37, No. 3, pp. 79-94.
- Uchimura, T., Tatsuoka, F., Tateyama, M., and Koga, T. (1998). “Preloaded-prestressed geogrid-reinforced soil bridge pier.” *Proceedings of the 6th International Conference on Geosynthetics*, Atlanta, Georgia, March 1998, Vol. 2, pp. 565-572.
- Vidal, H., 1969, “La Terre Armée.” *Annales de l’Institut Technique du Bâtiment et des Travaux Publics*, Materials, Vol. 38, No. 259-260, pp. 1-59.
- Won, G.W., Hull, T., and De Ambrosis, L. (1996). “Performance of a geosynthetic segmental block wall structure to support bridge abutments.” *Earth Reinforcement*, Ochiai, Yasufuku and Omine (eds), Balkema, pp. 543-549.
- Zornberg, J.G., Sitar, N., and Mitchell, J.K., 1998a, “Performance of Geosynthetic Reinforced Slopes at Failure.” *Journal of Geotechnical and Geoenvironmental Engineering*, ASCE, Vol. 124, No.8, pp. 670-683.
- Zornberg, J.G., Sitar, N., and Mitchell, J.K., 1998b, “Limit Equilibrium as a Basis for Design of Geosynthetic Reinforced Slopes.” *Journal of Geotechnical and Geoenvironmental Engineering*, ASCE, Vol. 124, No.8, pp. 684-698.
- Zornberg, J.G., Sitar, N., and Mitchell, J.K., 2000, Closure on discussion to “Limit Equilibrium as a Basis for Design of Geosynthetic Reinforced Slopes.” *Journal of Geotechnical and Geoenvironmental Engineering*, ASCE, Vol. 126, No. 3, pp. 286-288.

**ZORNBERG • ADVANCES IN REINFORCED SOIL TECHNOLOGY**

- Zornberg, J.G., and Leshchinsky, D., 2001, “Comparison of International Design Criteria for Geosynthetic-Reinforced Soil Structures.” *Geosynthetics and Earth Reinforcement*, H. Ochiai, J. Otani, and Y. Miyata (Editors), ISSMGE-TC9, pp. 106-117.
- Zornberg, J.G. (2002) “Discrete framework for limit equilibrium analysis of fibre-reinforced soil”, *Géotechnique* 52(8): pp. 593–604.

**ZORNBERG • ADVANCES IN REINFORCED SOIL TECHNOLOGY**

Table 1. Summary of Guidelines on Selection of Soil Shear Strength Parameters for Geosynthetic-Reinforced Soil Design

<b>Method/Agency</b>	<b>Shear Strength Parameters</b>	<b>Reference</b>
Jewell's Method	Residual	Jewell (1991)
Leshchinsky and Boedeker's method	Residual	Leshchinsky and Boedeker (1989)
Queensland DOT, Australia	Residual	RTA (1997)
New South Wells, Australia	Residual	QMRD (1997)
Bureau National Sols-Routes (draft French Standard)	Residual	Gourc et al. (2001)
Federal Highway Administration (FHWA), AASHTO	Peak	Elias et al. (2001), AASHTO 1996
National Concrete Masonry Association	Peak	NCMA (1997, 1998)
GeoRio, Brazil	Peak	GeoRio (1989)
Canadian Geotechnical Society	Peak	Canadian Geotechnical Society (1992)
German Society of Soil Mechanics and Geotechnical Engineering	Peak	EBGEO (1997)
Geotechnical Engineering Office, Hong Kong	Peak	GCO (1989), GEO (1993)
Public Works Research Center, Japan	Peak	Public Works Research Center (2000)
British Standards, United Kingdom	Peak	British Standard Institution (1995)
Leshchinsky's hybrid method	Hybrid	Leshchinsky (2001)

**ZORNBERG • ADVANCES IN REINFORCED SOIL TECHNOLOGY**

Table 2 Summary of soil properties

Soil type	Soil 1	Soil 2
USCS classification	SP	CL
LL %	-	49
PL %	-	24
IP %	-	25
% Fines	1.4	82.6

Table 3 Summary of fiber properties

	SP tests	CL tests
Linear density (denier)	1000 & 360	2610
Fiber content (%)	0.2 & 0.4	0.2 & 0.4
Length of fibers (mm)	25 & 51	25 & 51
Type of fiber	fibrillated & tape	fibrillate d

Table 4 Summary of parameters used in the prediction

	$\alpha$	$\phi$ (°)	$c$ (kPa)	$c_{i,c}$	$c_{i,\phi}$
Soil 1	1.0	34.3	6.1	0.8	0.8
Soil 2	1.0	31.0	12.0	0.8	0.8

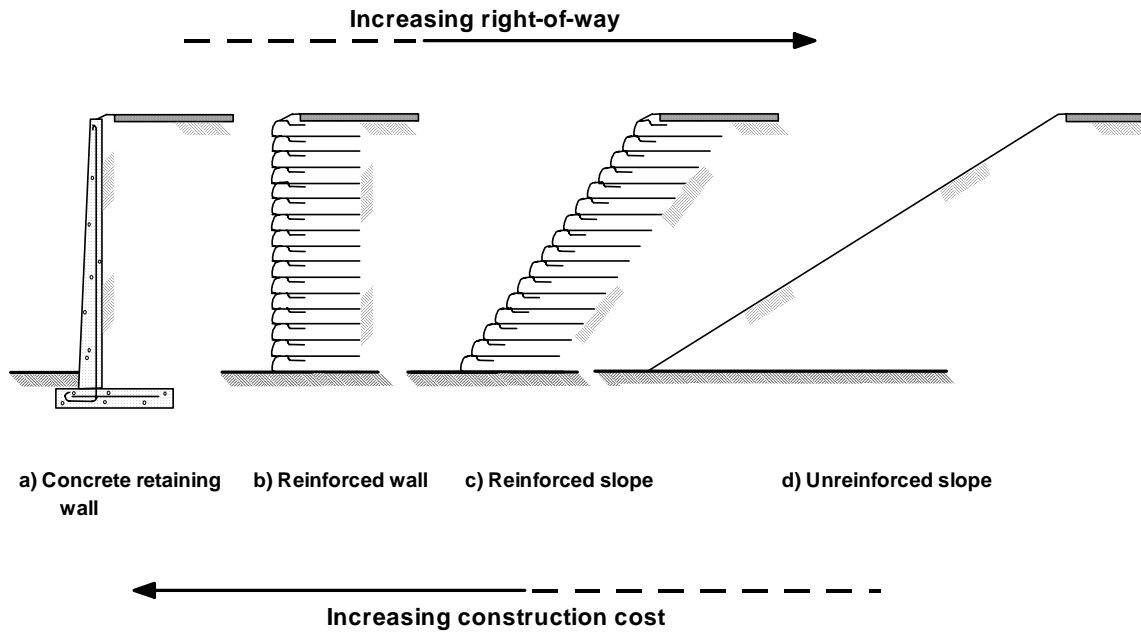


Figure 1. Reinforcement function of geosynthetics used to optimize the design of earth retaining structures.

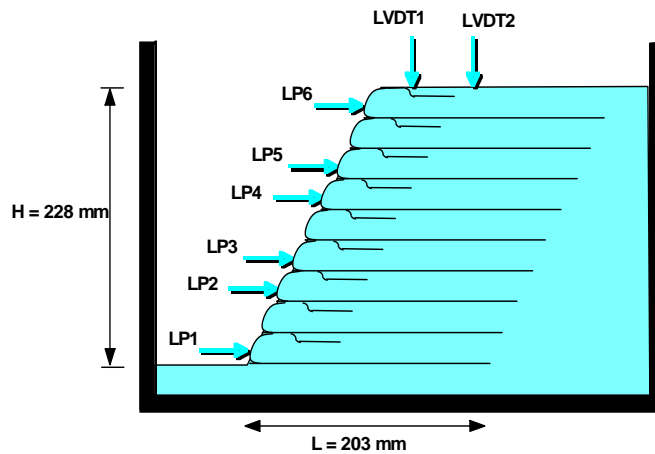


Figure 2. Typical centrifuge model.

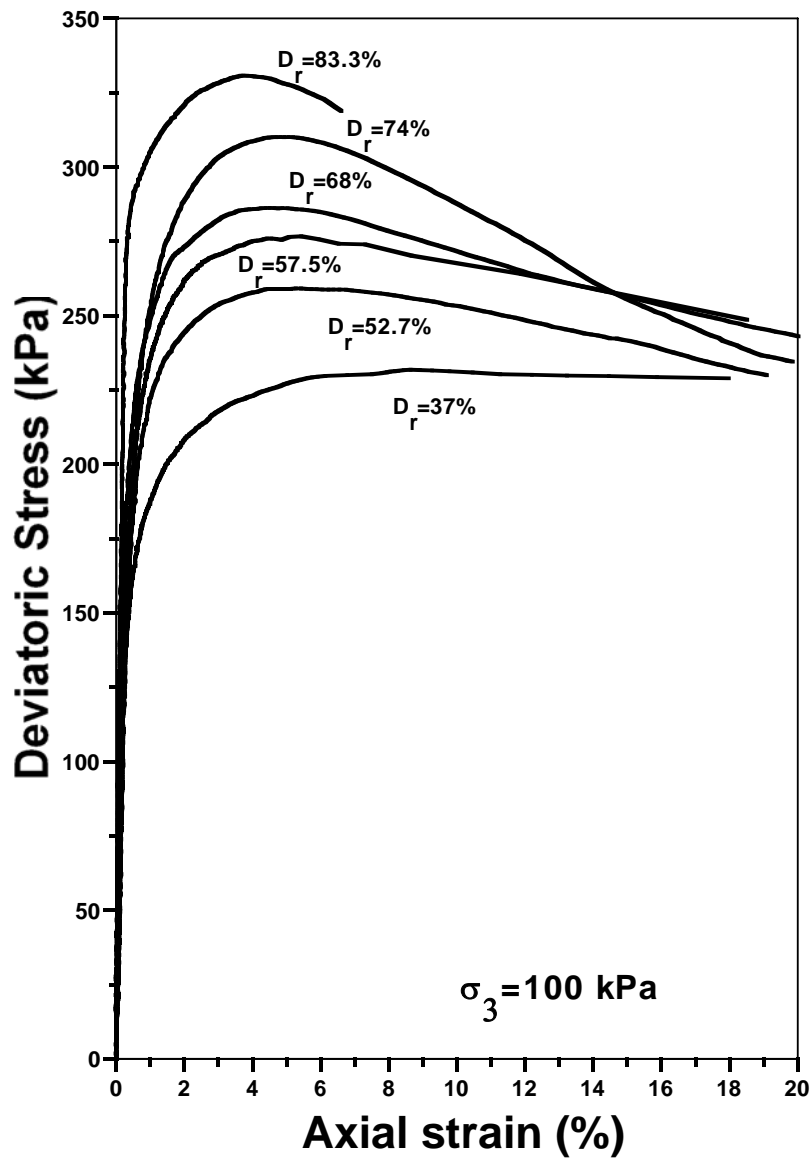


Figure 3. Stress strain behavior of Monterey No. 30 sand pluviated at different relative densities and tested in triaxial compression under the same confinement

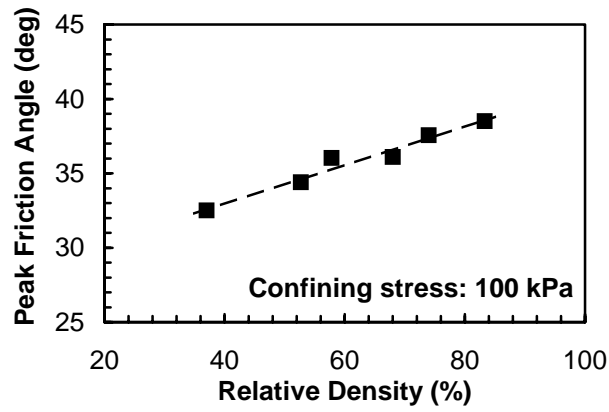


Figure 4. Friction angle for Monterey No. 30 sand obtained from triaxial testing at different relative densities.

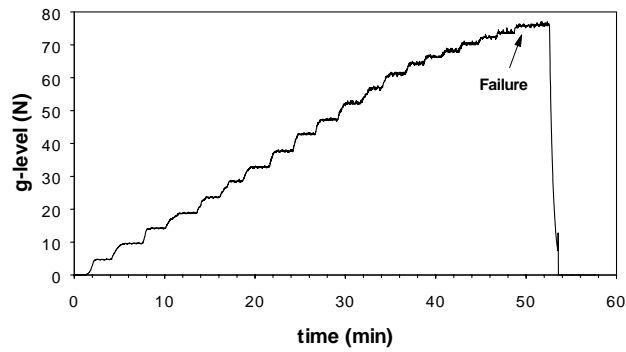


Figure 5. G-level (N) versus time during centrifuge testing.

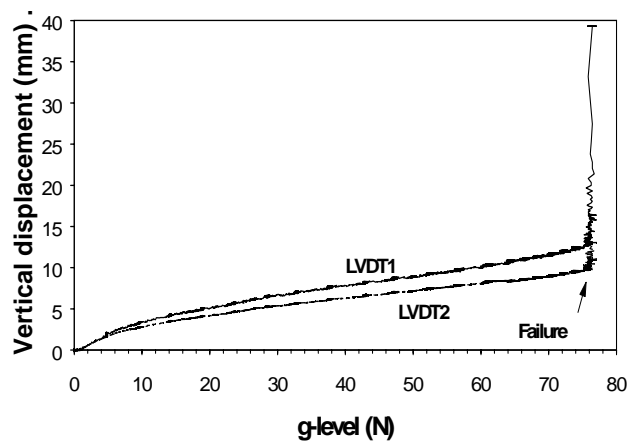


Figure 6. Settlements at the crest of a reinforced slope model.

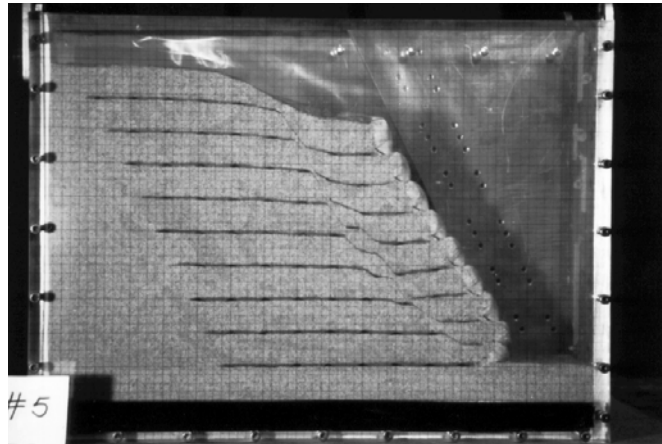


Figure 7. Failed geotextile-reinforced slope model.

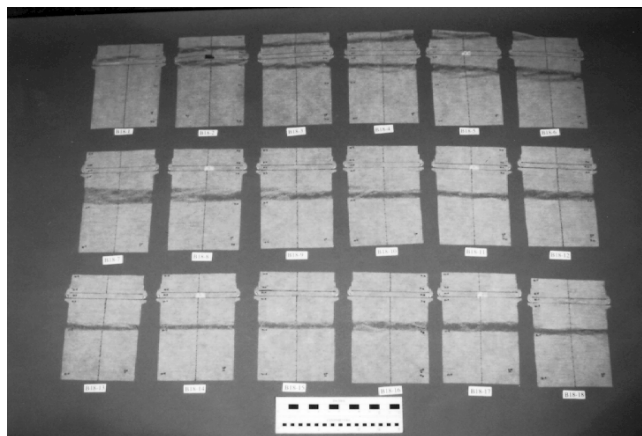


Figure 8. Geotextile reinforcements retrieved after testing.

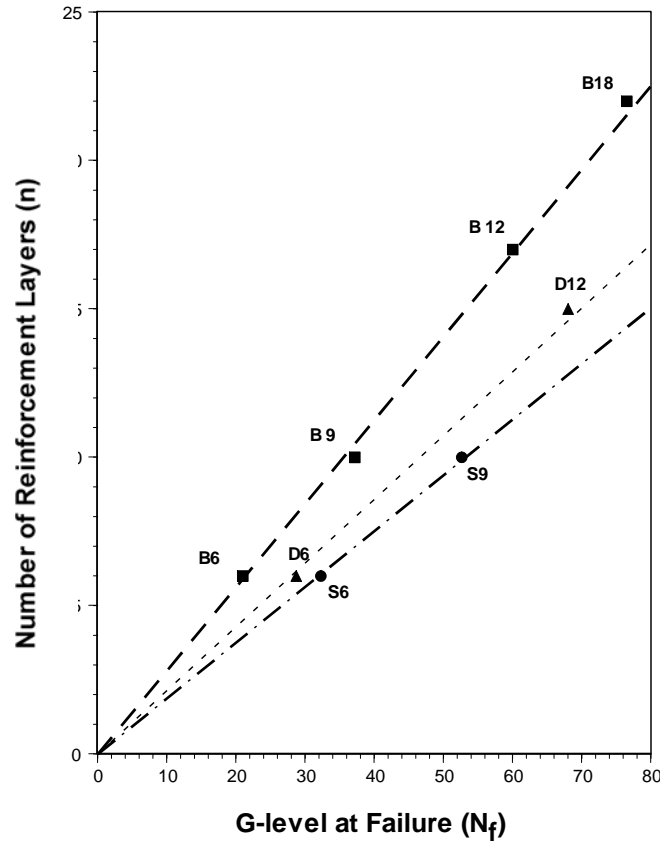


Figure 9. G-level at failure for the centrifuge models.

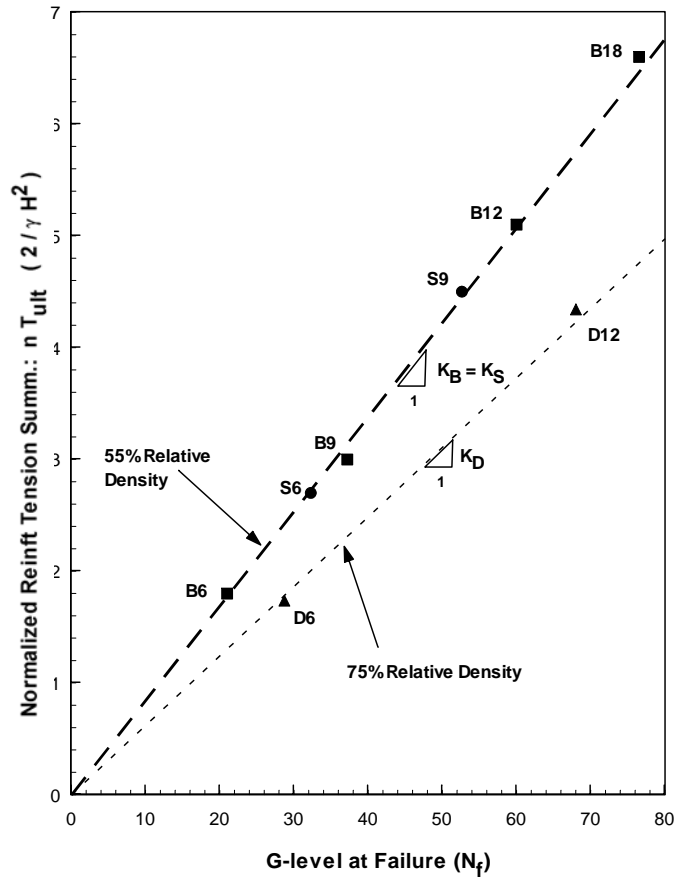


Figure 10. Normalized Reinforcement Tension Summation (RTS) values from centrifuge test results.



Figure 11. View of the Founders/Meadows GRS bridge abutments near Denver, Colorado.

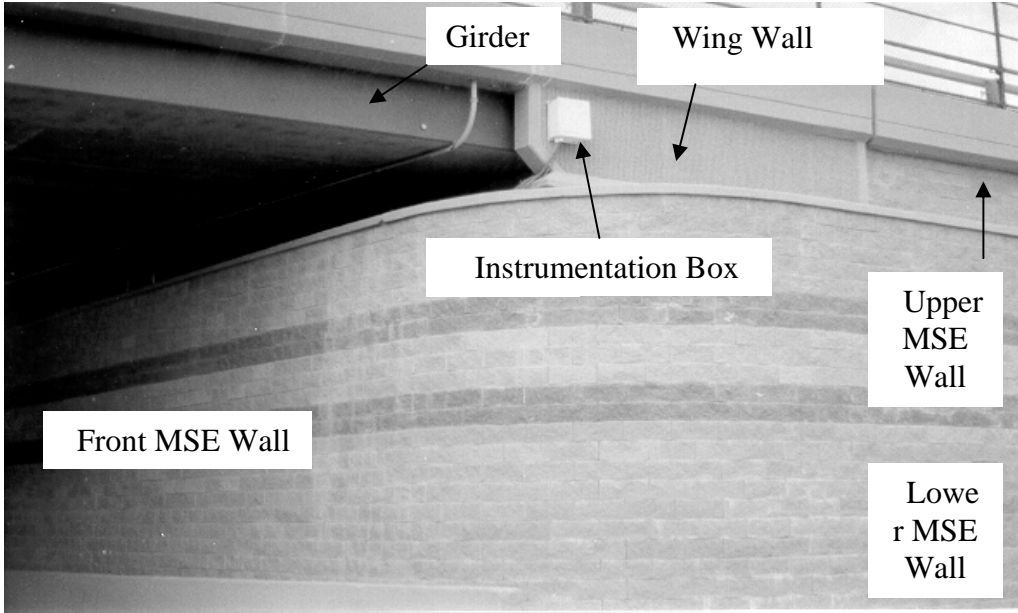


Photo 12. View of the Southeast side of the completed Founders/Meadows bridge abutment.

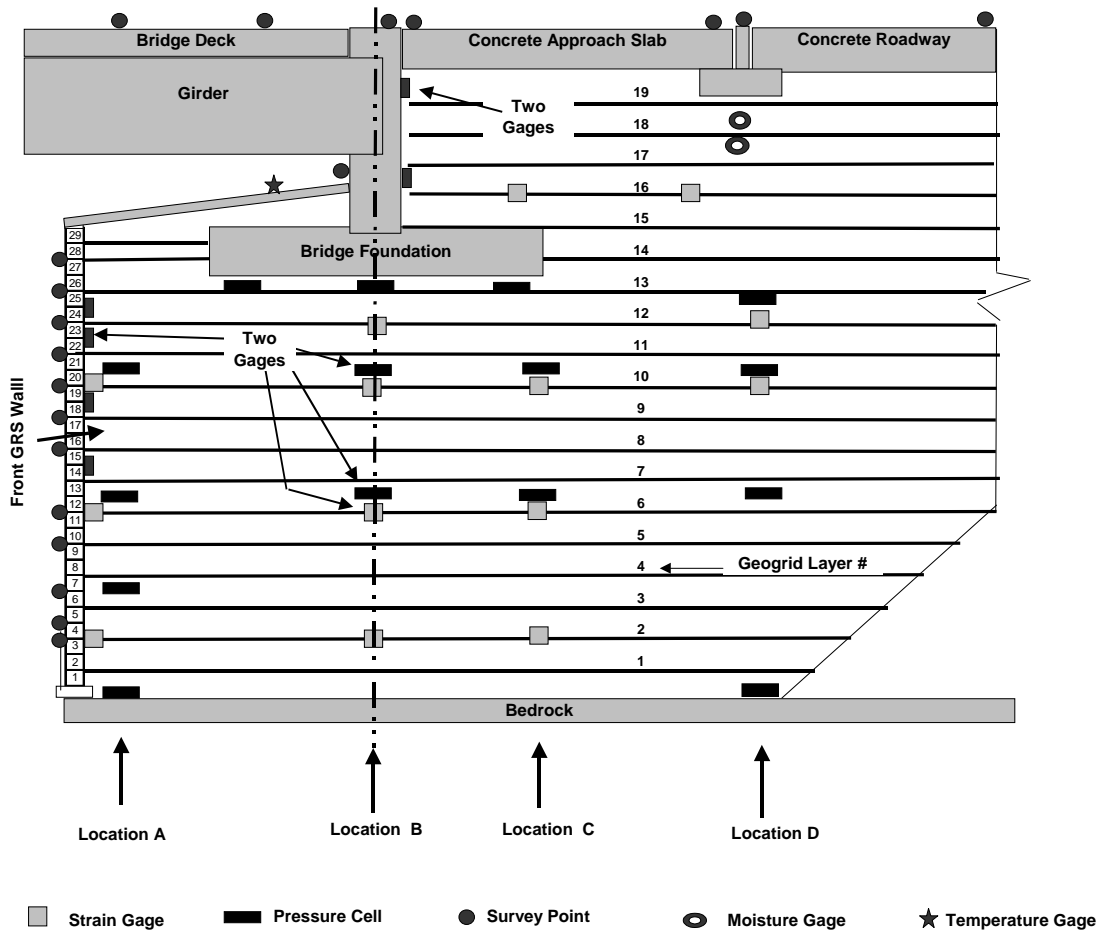


Figure 13. Instrumentation plan of Phase II structure.

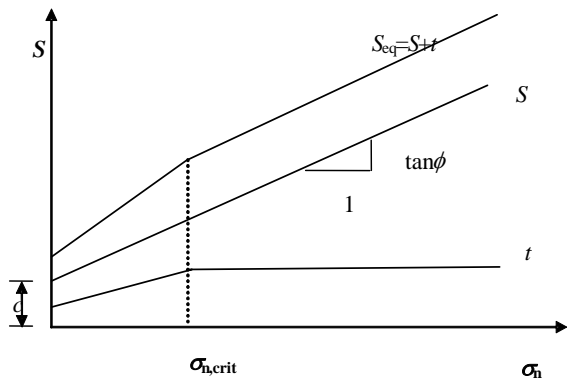


Figure 14 Representation of the equivalent shear strength according to the discrete approach

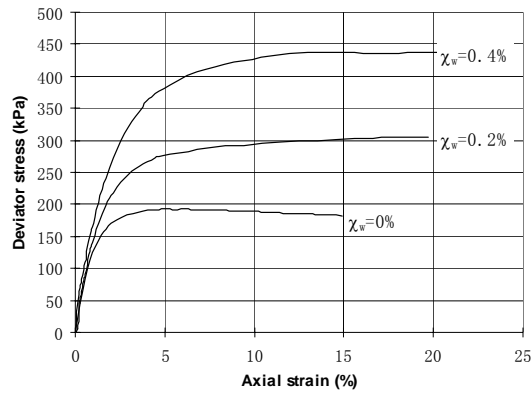


Figure 15. Stress-strain behavior of specimens prepared using  $w=0, 0.2$  and  $0.4\%$  with  $l_f = 25$  mm fibers (360 denier),  $\sigma_3=70$  kPa, Soil 1

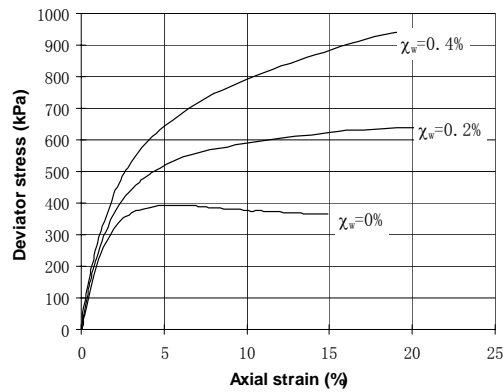


Figure 16 Stress-strain behavior of specimens prepared using  $w=0, 0.2$  and  $0.4\%$  with  $l_f = 25$  mm fibers (360 denier),  $\sigma_3=140$  kPa, Soil 1

ZORNBERG • ADVANCES IN REINFORCED SOIL TECHNOLOGY

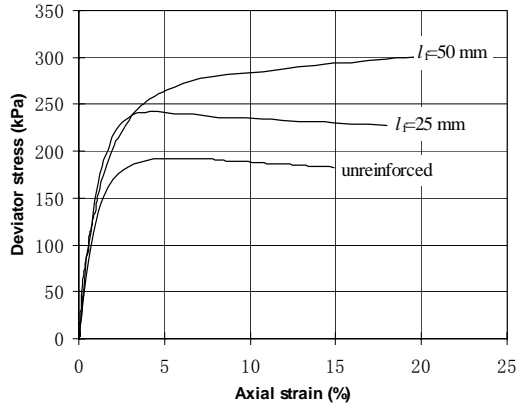


Figure 17 Stress-strain behavior of specimen prepared using  $\chi_w=0.2\%$ , with  $l_f=25$  mm and 50 mm fibers (1000 denier),  $\sigma_3=70$  kPa, Soil 1

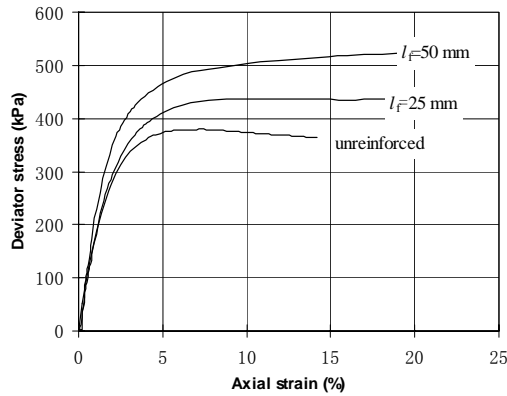


Figure 18 Stress-strain behavior of specimen prepared using  $\chi_w=0.2\%$ , with  $l_f=25$  mm and 50 mm fibers (1000 denier),  $\sigma_3=140$  kPa, Soil 1

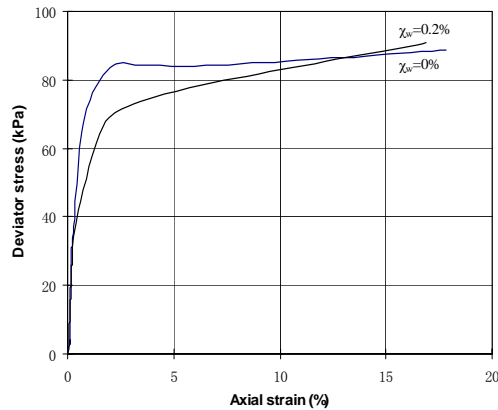


Figure 19 Stress-strain behavior of specimens prepared using  $\chi_w=0, 0.2\%$ , with  $l_f=50$  mm fibers (2610 denier),  $\sigma_3=98$  kPa, Soil 2

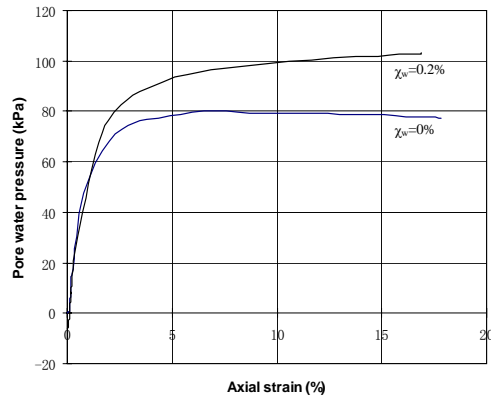


Figure 20 Excess pore water pressure of specimens prepared using  $\chi_w = 0, 0.2\%$ , with  $l_f = 50$  mm fibers (2610 denier),  $\sigma_3 = 98$  kPa, Soil 2

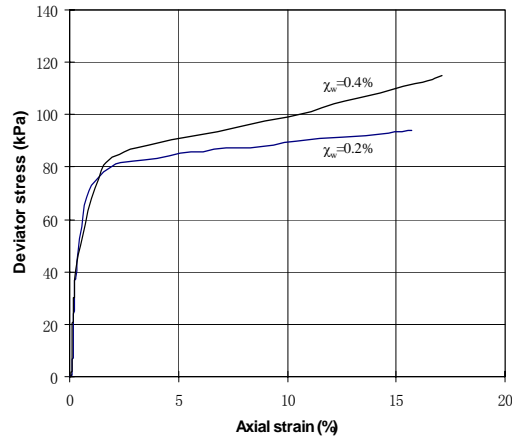


Figure 21 Stress-strain behavior of specimens prepared using  $\chi_w = 0.2, 0.4\%$ , with  $l_f = 25$  mm fibers (2610 denier),  $\sigma_3 = 116$  kPa, Soil 2

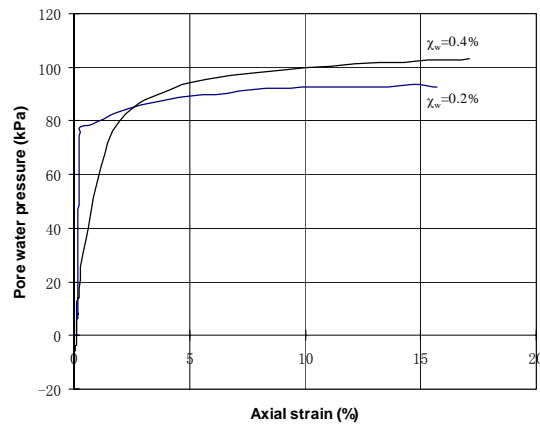


Figure 22 Excess pore water pressure of specimens prepared using  $\chi_w = 0.2, 0.4\%$ , with  $l_f = 25$  mm fibers (2610 denier),  $\sigma_3 = 116$  kPa, Soil 2

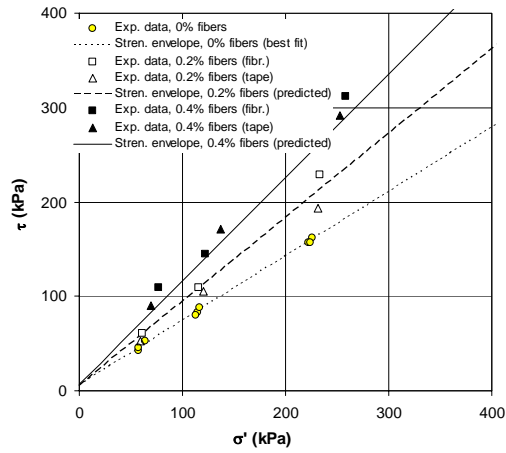


Figure 23 Comparison between predicted and experimental shear strength results for specimens reinforced at  $\chi_w=0$ , 0.2%, 0.4% with 25 mm-long fibers (360 denier), Soil 1

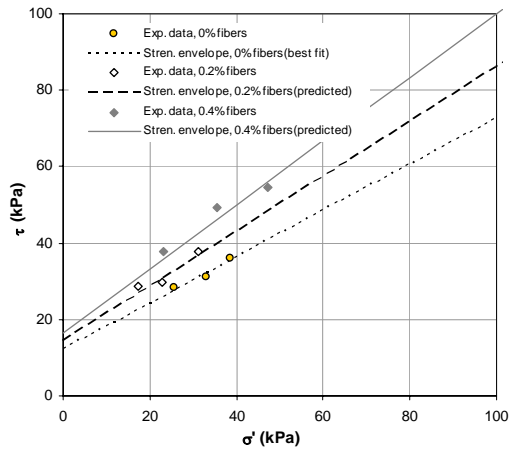


Figure 24 Comparison between predicted and experimental shear strength results for specimens reinforced at  $\chi_w=0$ , 0.2%, 0.4% with 50 mm-long fibers (2610 denier), Soil 2

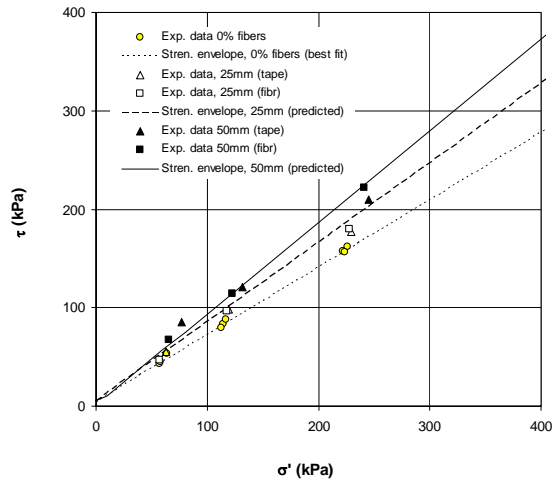


Figure 25 Comparison between predicted and experimental shear strength results for specimens reinforced at  $\chi_w = 0.2\%$ , with 25 mm-long and 50 mm-long fibers (1000 denier), Soil 1

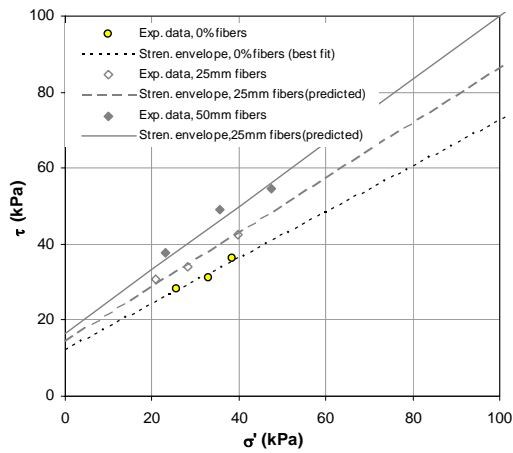


Figure 26 Comparison between predicted and experimental shear strength results for specimens reinforced at  $\chi_w = 0.4\%$ , with 25 mm-long and 50 mm-long fibers (2610 denier), Soil 2

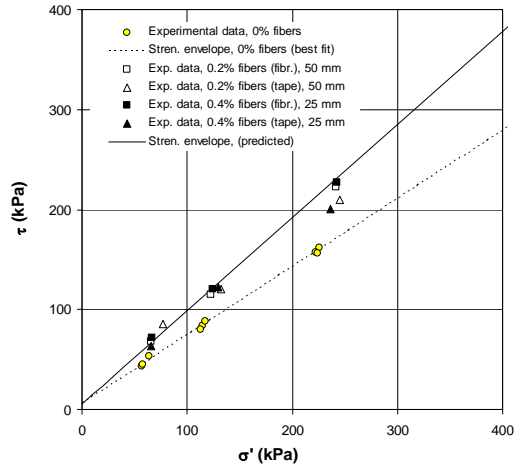


Figure 27 Consolidated shear strength results for specimen reinforced with 50 mm-long fibers (1000 denier) placed at  $\chi_w = 0.2\%$  and 25 mm fibers placed at  $\chi_w = 0.4\%$ , Soil 1

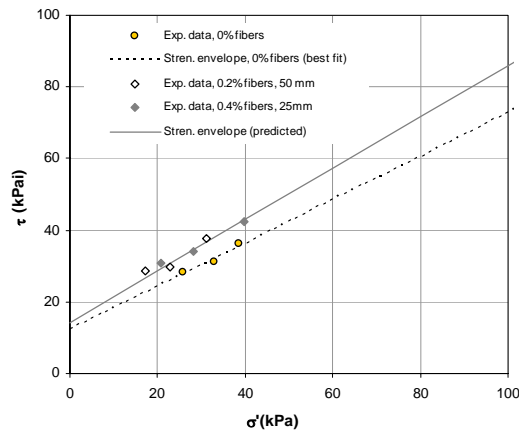


Figure 28 Consolidated shear strength results for specimen reinforced with 50 mm-long fibers (2610 denier) placed at  $\chi_w = 0.2\%$  and 25 mm fibers placed at  $\chi_w = 0.4\%$ , Soil 2

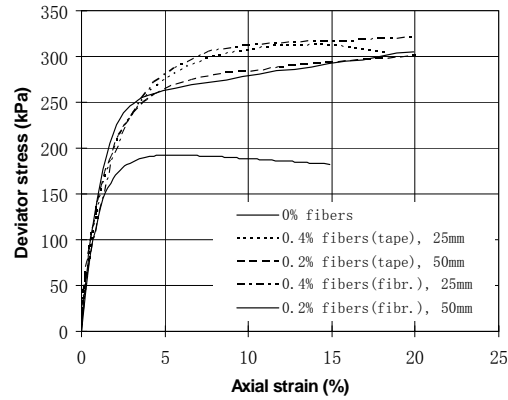


Figure 29 Comparison between stress-strain behavior for specimen reinforced with 50mm fibers (1000 denier) placed at  $\chi_w=0.2\%$  and 25 mm fibers placed at  $\chi_w=0.4\%$ ,  $\sigma_3=70$  kPa